International Journal of Nanomedicine

Dovepress
open access to scientific and medical research

Open Access Full Text Article

ORIGINAL RESEARCH

ROS-Generating Amine-Functionalized Magnetic Nanoparticles Coupled with Carboxymethyl Chitosan for pH-Responsive Release of Doxorubicin

Sreekanth Reddy Obireddy[1,2], Wing-Fu Lai[2]

[1]Department of Chemistry, Sri Krishnadevaraya University, Anantapur, 515003, India; [2]Ciechanover Institute of Precision and Regenerative Medicine, The Chinese University of Hong Kong (Shenzhen), Shenzhen, 518172, People's Republic of China

Correspondence: Wing-Fu Lai, Ciechanover Institute of Precision and Regenerative Medicine, The Chinese University of Hong Kong (Shenzhen), Shenzhen, 518172, People's Republic of China, Email rori0610@graduate.hku.hk

Purpose: Magnetic nanoparticles have been used in diverse pharmaceutical applications because they can potentially be used to target specific sites. In the present work, a new type of nanocomposites is designed as a carrier of controlled bioactive agent delivery.

Methods: Amine-functionalized magnetic nanoparticles (amine-MNPs) are coupled with carboxymethyl chitosan (CMC) to generate the nanocomposites, namely MNPs-CMC, which can be further loaded with doxorubicin (DOX) to produce MNPs-CMC-DOX. The generated nanocomposites are characterized by using various techniques (including FTIR, ^{1}H-NMR, DSC, TGA, SEM, TEM and XRD). In vitro drug release studies are conducted in PBS with different pH values (1.2 and 6.8) at different temperatures (25°C and 37°C). The toxicity of the nanocomposites is tested in MCF-7 and 3T3 cells. The ROS-generating capacity of the nanocomposites is determined in treated cells using 2',7'-dichlorodihydrofluorescein diacetate.

Results: The structures of MNPs, CMC, and nanocomposites are confirmed by FTIR, XRD, and ^{1}H-NMR data reveals the formation of CMC from chitosan (CS). The size of MNPs is estimated by TEM to be around 25 nm. After conjugation with CMC, the size of the nanocomposites increases to 46–57 nm. Based on the release profiles of MNPs-CMC-DOX, our nanocomposites are pH-responsive. In addition, our nanocomposites show reactive oxygen species (ROS)-generating capacity and cell type-dependent toxicity.

Conclusion: Our nanocomposites show high potential for use in bioactive agent delivery. Along with their ROS-generating capacity, they warrant further development as pH-responsive carriers for therapeutic applications.

Keywords: nanocomposites, drug delivery, controlled release, biocompatibility

Introduction

Metal nanoparticles show physical and chemical properties that are different from their corresponding bulk materials.[1,2] For this, metal nanoparticles show high toxicity even though the same metal exhibits inertness in its bulk form.[3,4] An earlier study has found that gold nanoparticles (with the diameter of around 50 nm) can result in a range of toxicological features upon administration in vivo.[5] A similar observation has also been reported by Park et al,[6] who have noted that intratracheal and intravenous administration of platinum nanoparticles in vivo can elicit inflammation, causing an increase in cytokine generation and in the immunoglobulin E (IgE) concentration. When the size of the nanoparticles is small enough to enter the nucleus, the genetic material of the cell may even be affected.[7] More recently, Alarifi et al reported that nickel nanoparticles cause oxidative stress in cells by stimulating the formation of reactive oxygen species.[8] An increase in the level of membrane lipid peroxidation (LPO) and the amount of ROS, and a decrease in intracellular glutathione concentrations, are observed in vitro after exposure to metal nanoparticles.[9] This sheds light on the possibility of using nanoparticles as ROS-generating materials for therapeutic purposes. This possibility has been corroborated by the case of Fe_3O_4 (magnetite) and γ-Fe_2O_3 (maghemite) nanoparticles, which have recently been extensively exploited for biomedical applications, including magnetic resonance imaging (MRI) and hyperthermia.[10–15] For the latter, malignant tumours are more sensitive to heat than normal tissues at around 41–47°C. Once magnetic metal nanoparticles enter

Received: 16 September 2021
Accepted: 5 December 2021
Published: 8 February 2022

Graphical Abstract

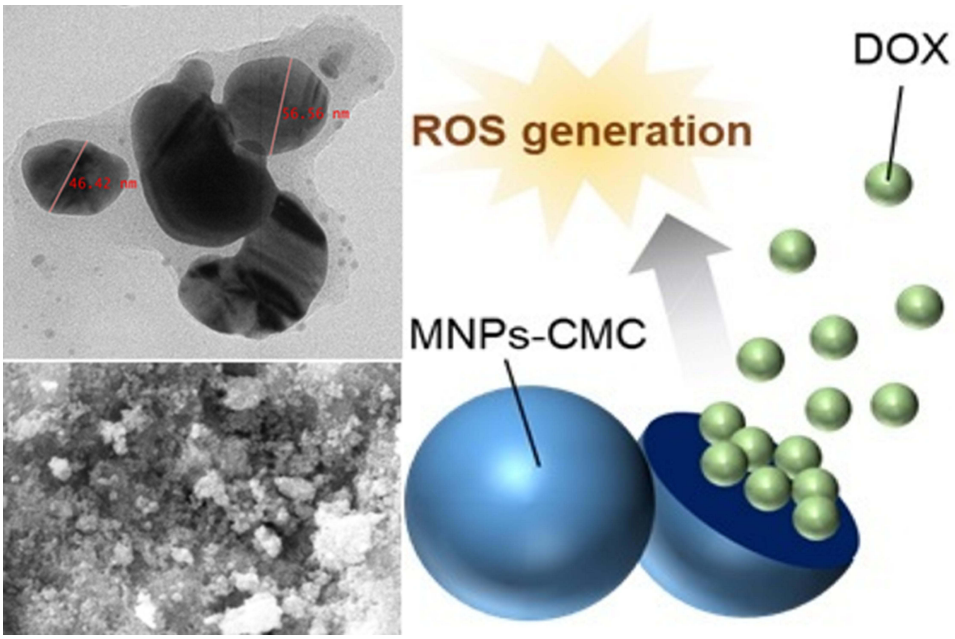

cancer cells and are subjected to an alternate magnetic field, they absorb energy, with the relaxation effect producing a heating effect to cause the death of the cancer cells.[16–18] In recent years, researchers have attempted to combine magnetic nanoparticles with a variety of anticancer agents [such as 5-fluorouracil,[19] paclitaxel,[20] and doxorubicin (DOX)[21]] for cancer treatment.

Apart from metal nanoparticles, natural biodegradable polymers are advancing the research front in bioactive agent delivery.[22–25] For instance, chitin and its derivatives have been employed to administer drugs or nutritional supplements.-[26] One of the most widely studied derivatives of chitin is chitosan (CS),[27–30] whose various favourable properties (including the film-forming ability, the antibacterial activity, the ability to interact with different substances, and the high solubility across a wide pH range) enabling it and its derivatives to be adopted not only in wound therapy[31] and cancer treatment[32,33] but also in immunological modulation.[34] In this study, we combine carboxymethyl CS (CMC), which is a biocompatible and biodegradable polymer possessing free hydroxyl, amino, and carboxylic groups to cross-link with diverse functional groups found in bioactive compounds,[35] with ROS-generating magnetic metal nanoparticles to fabricate a bioactive carrier for pH-responsive release of the loaded agent.

Materials and Methods

Materials

CS, ammonium hydroxide, ferrous chloride tetrahydrate ($FeCl_2.4H_2O$), ferric chloride hexahydrate ($FeCl_3.6H_2O$), 1-ethyl-3-[3-dimethylaminopropyl]carbodiimide hydrochloride (EDC), N-hydroxysuccinimide (NHS) and ethylenediamine were obtained from Sigma-Aldrich (St. Louis, MO, USA). Sodium hydroxide (NaOH), isopropanol, methanol, ethanol, glacial acetic acid, and monochloroacetic acid were purchased from SD Fine Chemicals Ltd. (Mumbai, India). DOX was provided by Aspiro Pharma (Telangana, India).

Synthesis of Amine-Functionalized Magnetic Nanoparticles (Amine-MNPs)

Synthesis of amine-MNPs was performed as previously reported,[36] with some modifications made for incorporating amine groups onto the nanoparticle surface. In 100 mL of water, 0.6 g of $FeCl_2.4H_2O$ and 1.6 g of $FeCl_3.6H_2O$ were

added, followed by stirring at 500 rpm for 60 min under a nitrogen atmosphere. After that, 40 mL of a 30% (w/v) ammonium hydroxide solution and 40 mL of ethylenediamine were added. The reaction mixture was stirred at 60°C for 60 min. The black precipitates formed were isolated using a magnet, washed with distilled water, air-dried, and sealed in an airtight container for subsequent use.

Synthesis of CMC

CMC was synthesized as previously described.[37] In brief, in 100 mL of isopropanol, 6 g of chitosan was added. After being stirred at 300 rpm for 30 min, 30 mL of a 10M NaOH solution was added dropwise, followed by the addition of 15 mL of a 10% (v/v) monochloroacetic acid solution. The reaction mixture was stirred at 50°C for 6 h. 100 mL of methanol was then added. Neutralization of the reaction mixture was performed using glacial acetic acid. The slurry was filtered. The solid obtained was thoroughly washed using 80% (v/v) ethanol and air-dried.

Synthesis of MNPs-CMC and MNPs-CMC-DOX Nanocomposites

0.2 g of CMC was dissolved in 10 mL of water. 100 mg of amine-functionalized MNPs was added, followed by sonication for 15 min. 0.1 g of 1-ethyl-3-[3-dimethylaminopropyl]carbodiimide hydrochloride (EDC) and 0.1 g of N-hydroxysuccinimide (NHS) were added. The reaction mixture was stirred for 3 h.100 mg of DOX was then added, followed by stirring at ambient conditions for 6 h. The reaction mixture was centrifuged at 10000 rpm for 5 min. The obtained MNPs-CMC-DOX nanocomposites were washed with ethanol and dried at 40°C in an oven. The same procedure was adopted to generate MNPs-CMC nanocomposites but DOX was not added during the process.

Determination of Structural and Physico-Chemical Properties

Structural characterization of CMC and amine-MNPs was performed using proton nuclear magnetic resonance (^{1}H-NMR) spectroscopy (400 MHz) (Bruker Avance III; Bruker, USA), Fourier-transform infrared (FTIR) spectroscopy (Bomem MB-3000; ABB Corporate, Zurich, Switzerland), and X-ray diffraction (XRD) spectroscopy (Ultima IV; Rigaku, Japan). The structures of MNPs-CMC and MNPs-CMC-DOX were examined by using an FTIR spectrometer (Bomem MB-3000; ABB Corporate, Zurich, Switzerland). Spectra were obtained at a resolution of 2 cm^{-1}, and reported as an average of 16 scans. Differential scanning calorimetry (DSC) and thermogravimetric analysis (TGA) (DSC-SP; Rheometric Scientific, UK) were performed by heating the sample at a heating rate of 10°C/min under a nitrogen atmosphere from 40°C to 600°C. The morphological features of amine-MNPs and MNPs-CMC-DOX were captured using scanning electron microscopy (SEM) (JEOL JSM 6100; JEOL, Japan). Transmission electron microscopy (TEM) (JEOL JEM 2100; JEOL, Japan) and dynamic light scattering (DLS) (Nano-S90; Malvern, UK) were used to determine the size of amine-MNPs and MNPs-CMC-DOX.

Evaluation of the Encapsulation Efficiency (EE)

10 mg of MNPs-CMC-DOX was dispersed in 10 mL of phosphate buffer saline (PBS) to which 0.5 mL of ethanol was added. The dispersion was agitated in the dark under ambient conditions for 24 h. After sonicating the dispersion for 10 min, the nanocomposites were retrieved by centrifugation and crushed in PBS. The concentration of DOX in the filtrate obtained was analysed by using a UV-Vis spectrometer (UV 3000+; Labindia, India) at a wavelength of 479.2 nm. The EE was determined using the following formula:[38]

$$\text{EE}\ (\%)\ = \frac{\text{A}_f}{\text{A}_d} \times\ 100\%$$

where A_f is the amount of DOX in the filtrate and A_d is the total amount of DOX added during MNPs-CMC-DOX fabrication.

Determination of the Kinetics of Agent Release

To study the release patterns of MNPs-CMC-DOX, dissolution analysis was conducted using a dissolution tester (DS8000; Labindia, India) in PBS with different pH values (1.2 and 6.8) at different temperatures (25°C and 37°C),

with the rotation speed set to 50 rpm. 30 mg of MNPs-CMC-DOX was put into a dialysis bag and dispersed in 300 mL of PBS. At regular time intervals, 3 mL of PBS was sampled and replaced with the same volume of fresh PBS. The concentration of DOX in the sample was analysed by using a UV-Vis spectrometer (UV 3000+; Labindia, India) at a wavelength of 479.2 nm. The release data obtained were fitted into various kinetics models (including the zero-order model, first-order model, Higuchi model, and Korsmeyer-Peppas model[39,40]) to identify the best fitted one.

Evaluation of the Cytotoxicity and ROS-Generating Capacity of the Nanocomposites

MCF7 cells and 3T3 fibroblasts were seeded into a 96 well plate, in which 200 µL of DMEM was added to each well. After incubating the plate at 37°C in a 5% CO_2 atmosphere for 24 h, the nanocomposites (MNPs-CMC and MNPs-CMC-DOX) were added to each well to reach a desired concentration (6.25, 12.5, 25, 50 and 100 µg/mL). The cells were treated with the nanocomposites at 37°C in a 5% CO_2 atmosphere for 24 h. After that, an MTT reagent was added to each well to reach the concentration of 0.5 mg/mL. The plate was incubated at 37°C for 3 h. The unreacted reagent was then aspirated. The violet crystals in each well were dissolved in 100 µL of DMSO. The colour intensity was measured by an ELISA reader at a wavelength of 570 nm. The ROS-generating capacity of the nanocomposites was determined using 2',7'-dichlorodihydrofluorescein diacetate (H_2DCFDA) as previously described.[41]

Results and Discussion

Structural Characterization of the Nanocomposites

Magnetic metal nanoparticles are synthesized, modified into amine-MNPs, and coupled with CMC. Upon being loaded with DOX, MNPs-CMC-DOX is obtained. Successful synthesis of CMC in this study is confirmed by using ^{1}H-NMR (Figure 1). The spectrum of CMC shows signals at 4.430 and 4.702 ppm. These signals are assigned to the two methyl protons of the carboxymethyl group and to the –OH proton at the C3 position, respectively. Similar signals have also been found by Bukzem et al,[37] who have characterized CMC using ^{1}H-NMR in an earlier study. The success of N-carboxymethylation is confirmed by the appearance of a signal at 3.703 ppm. This signal is attributed to the two protons of the carboxymethyl group bound to the nitrogen atom at the C2 position. To further confirm the successful generation of CMC and amine-MNPs (Figure 2), XRD spectroscopy is adopted. The XRD pattern of amine-MNPs shows peaks at 2θ of 30.3°, 35.7°, 43.4°, 54.2°, 57.3° and 62.9°. The peaks are assigned to the (220), (311), (400), (422), (511) and (440) planes (JCPDS card no. 19–0629), respectively. The XRD pattern of CMC shows peaks at 2θ of 20.32° and 27.84°, indicating the formation of CMC from chitosan is successful.

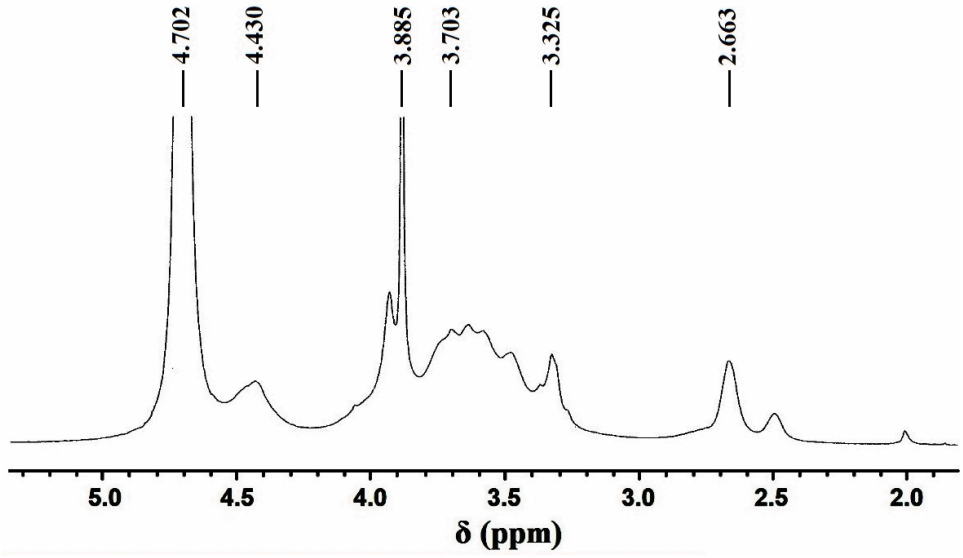

Figure 1 ^{1}H-NMR spectrum of CMC.

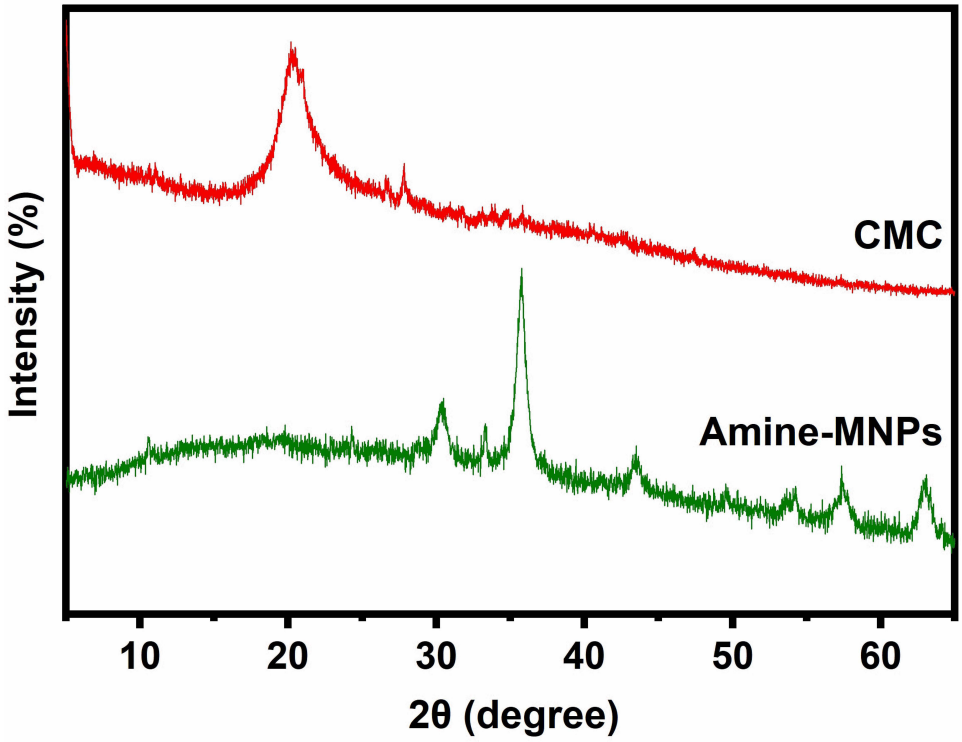

Figure 2 XRD patterns of CMC and amine-MNPs.

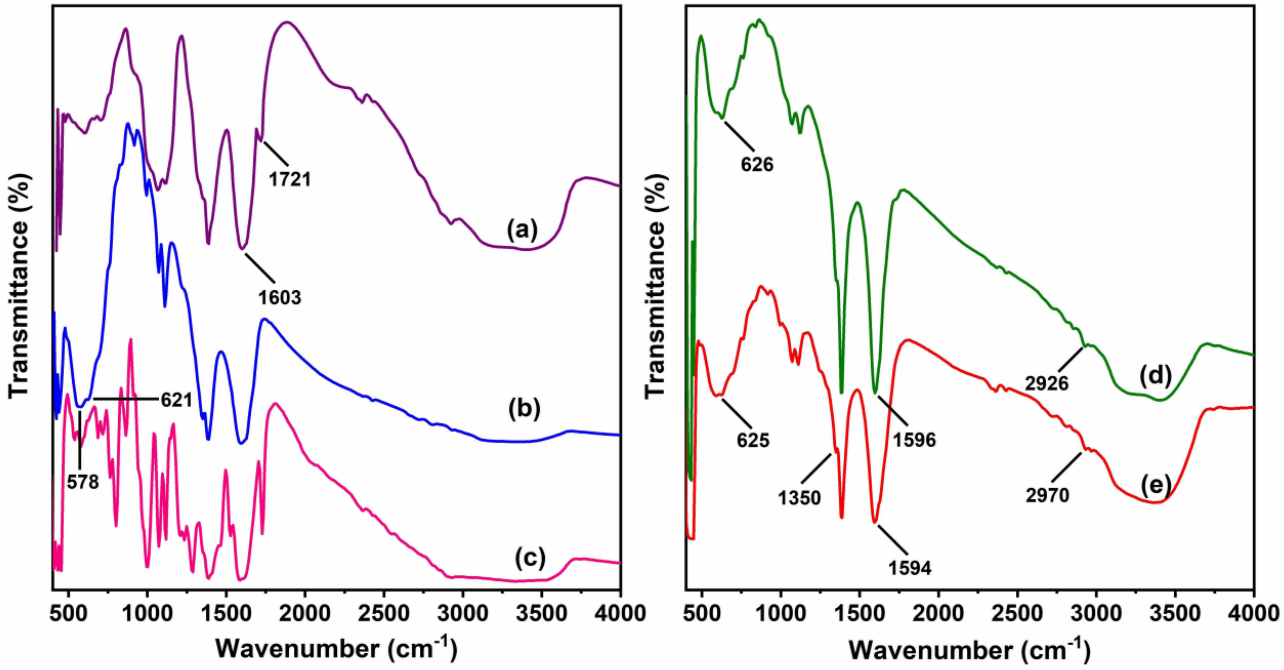

Figure 3 FTIR spectra of (a) CMC, (b) amine-MNPs, (c) DOX, (d) MNPs-CMC and (e) MNPs-CMC-DOX.

To investigate the interactions among amine-MNPs, CMC and DOX, FTIR analysis is performed (Figure 3). The spectrum of CMC shows peaks at 3207 cm^{-1} and 3433 cm^{-1}. These peaks are caused by –OH and –NH stretching vibrations, respectively. This is consistent with the observation made by Nivethaa et al in their study on CMC.[42] Peaks at 2923 cm^{-1} (due to C–H stretching vibrations), 1601 cm^{-1} (due to symmetric axial deformation of –COOH) and

1392 cm^{-1} (due to asymmetric axial deformation of –COOH) confirm the existence of carboxymethyl groups on chitosan. Peaks at 1064 cm^{-1} and 1111 cm^{-1} are assigned to C–O-C stretching vibrations, indicating the existence of carbonyl groups. The spectrum of amine-MNPs show peaks at 578 cm^{-1} and 624 cm^{-1} (due to stretching vibrations of Fe–O), 1595 cm^{-1} (due to bending vibrations of NH_2) and at around 3422 cm^{-1} (due to stretching vibrations of N–H). This suggests that amine groups are incorporated successfully onto the nanoparticle surface.

The spectrum of DOX shows peaks at 3325 cm^{-1} (due to stretching vibrations of O–H and N–H), 1731 cm^{-1} (due to stretching vibrations of C=O), 1388 cm^{-1} (due to bending vibrations of O–H), 1589 cm^{-1} (due to bending vibrations of N–H), 1072 cm^{-1} (due to stretching vibrations of C–O), 1288 cm^{-1} (due to stretching vibrations of C–N), 995 cm^{-1} (due to bending vibrations of C=C), and 802 cm^{-1} (due to bending vibrations of C–H). When comparing with the spectrum of CMC, a new peak is observed at 626 cm^{-1} in the spectrum of MNPs-CMC. This is a characteristic peak of amine-MNPs, indicating that the nanoparticles are successfully conjugated with CMC. Furthermore, the peak (1596 cm^{-1}) assigned to stretching vibrations of C=O is lowered in the spectrum of MNPs-CMC, suggesting that the C=O groups of CMC have interacted with the NH_2 groups of amine-MNPs. This confirms the formation of MNPs-CMC. On the other hand, peaks found in the spectrum of MNPs-CMC are found in the spectrum of MNPs-CMC-DOX, which, however, shows a new peak at 1350 cm^{-1}. This peak is assigned to C-O-C asymmetric stretching vibrations of DOX. Another new peak is found at 2970 cm^{-1}. It results from aromatic C-C stretching vibrations of DOX. The presence of it evidences that DOX is loaded successfully into MNPs-CMC.

Morphological Features and Size Distribution

TEM analysis of amine-MNPs and MNPs-CMC-DOX shows that the size of amine-MNPs increases from around 7–25 nm to 46–57 nm upon conjugation with CMC and upon the DOX loading process (Figure 4A and B). This is in good agreement with the observation made by Bhattacharya and coworkers,[43] who have reported an increase in the size of metal nanoparticles when the nanoparticles have been coated with the polymer matrix. The SAED patterns of amine-MNPs and MNPs-CMC-DOX display multiple diffuse polycrystalline rings (Figure 4C and D), indicating that the size of the nanocomposites is small. A similar observation has also been reported by an earlier study on the development of pH-sensitive superparamagnetic iron-oxide nanocomposites for drug delivery.[44] The small size of the nanocomposites is further confirmed by SEM (Figure 5A and B) and DLS (Figure 5C and D). Both techniques show that amine-MNPs and MNPs-CMC-DOX (Figure 5B) have a diameter in the nanoscale.

Thermal Properties

The thermal stability of DOX in the nanocomposites is studied using TGA (Figure 6). The TGA curve of amine-MNPs shows a weight loss in the temperature range from 40°C to 600°C. This is due to the loss of adsorbed moisture. The TGA curve of CMC shows a three-stage weight loss process. The first stage is from 40°C to 244°C, resulting in a weight loss of 28% due to the loss of adsorbed moisture. The second and third stages occur at 255–342°C and 356–600°C, leading to a weight loss of 26% and 13%, respectively. These two stages are the result of the degradation of the polymer backbone. A three-stage weight loss process is also observed in the TGA curve of DOX. The first stage occurs in the temperature range from 40°C to 196°C, leading to a weight loss of 1.4% due to the evaporation of adsorbed moisture. The second and third stages occur in the temperature range from 198°C to 261°C and from 267°C to 600°C, causing a weight loss of 26% and 21%, respectively, due to the decomposition of DOX. In the TGA curves of MNPs-CMC and MNPs-CMC-DOX, a two-stage weight loss is observed. MNPs-CMC-DOX starts to decompose at 182°C, which is slightly higher than the decomposition temperature of MNPs-CMC (165°C). Comparing with CMC alone, MNPs-CMC and MNPs-CMC-DOX are more thermally stable. This is attributed to the interactions between amine-MNPs and CMC.

To investigate the molecular dispersion of DOX and the phase change experienced by amine-MNPs during the fabrication of MNPs-CMC and MNPs-CMC-DOX, DSC is adopted (Figure 6). In the DSC pattern of DOX, a peak is found at 248°C. This is the melting peak of the drug.[45] This peak is, however, absent in the DSC pattern of MNPs-CMC-DOX, implying that DOX is dispersed evenly in the nanocomposites. The phase change from γ-Fe_2O_3 to α-Fe_2O_3 explains the appearance of an endothermic peak at 581°C in the DSC pattern of amine-MNPs. This peak is not found in

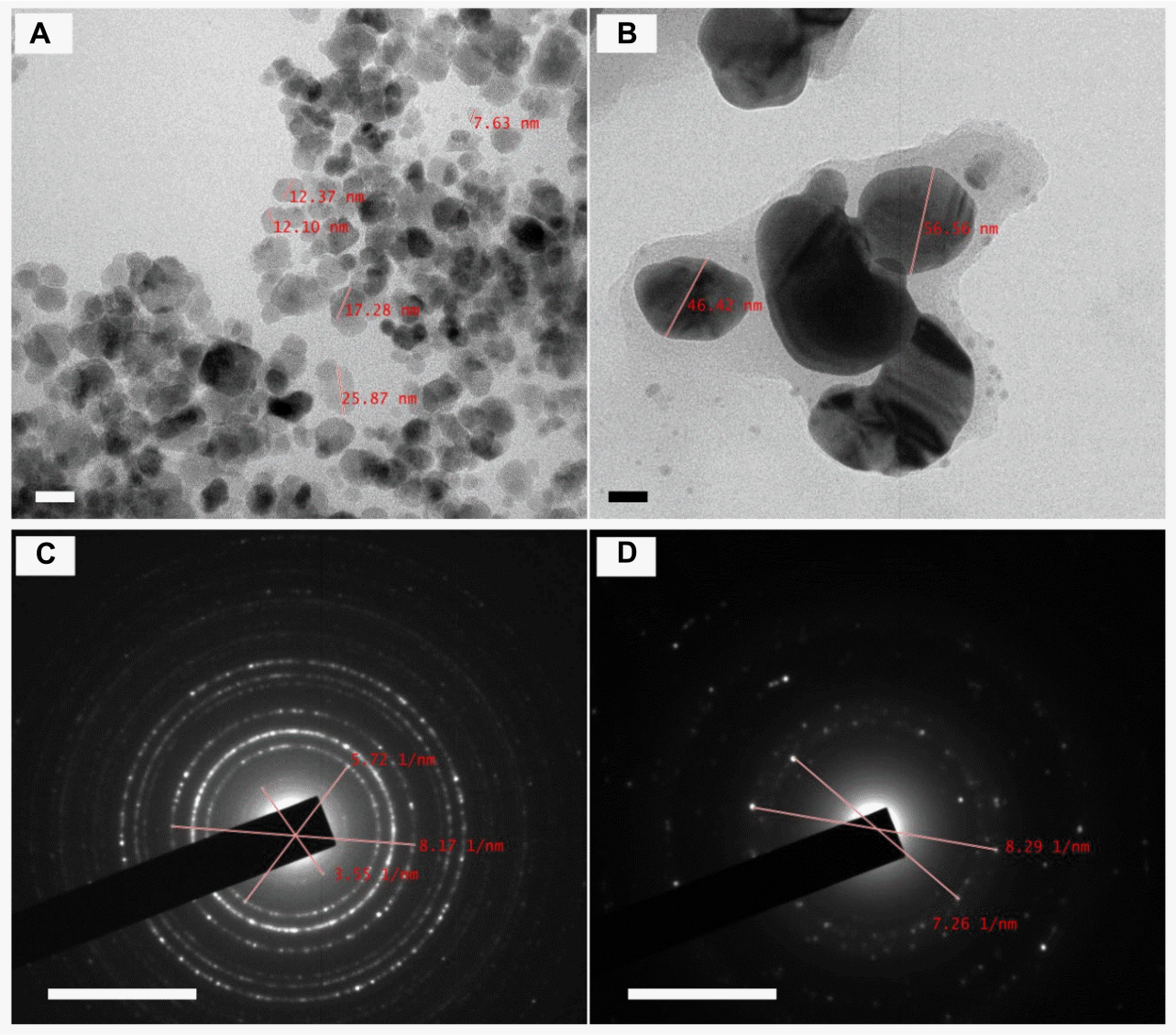

Figure 4 TEM images of (**A**) amine-MNPs and (**B**) MNPs-CMC-DOX. Scale bar = 20 nm. SAED patterns of (**C**) amine-MNPs and (**D**) MNPs-CMC-DOX. Scale bar = 51 nm.

the DSC pattern of MNPs-CMC-DOX. This is because amine-MNPs in MNPs-CMC-DOX are stabilized by the interactions between γ-Fe_2O_3 and CMC.[36]

Encapsulation and Release of the Loaded Agent

The EE of MNPs-CMC-DOX is estimated to be 54.2%. The release pattern of MNPs-CMC-DOX is examined at pH 1.2 and 6.8 at 37°C (Figure 7A and B). The release sustainability of the nanocomposites is maintained at both pH values. At pH 1.2, 35%, 48%, 67% and 74% of the loaded agent is released after 24 h, 48 h, 72 h and 96 h, respectively. These percentages drop to 30%, 44%, 61% and 70%, respectively, when the pH increases to 6.8. Such pH-responsiveness is explained by the swelling property of the polymer matrix. The unreacted amine groups in CMC are protonated at lower pH, thereby having repulsive interactions with the nearby positive charges. This disrupts the electrostatic interactions between DOX and the polymer matrix of CMC, leading to an increase in the rate of DOX release. A similar pattern of pH-responsive agent release is observed at 25°C. 72% of DOX is released after at pH 1.2 after 96 h but this percentage drops to 68% when the pH increases to 6.8, indicating that the swelling property of the polymer matrix is predominately due to pH but not temperature.[46]

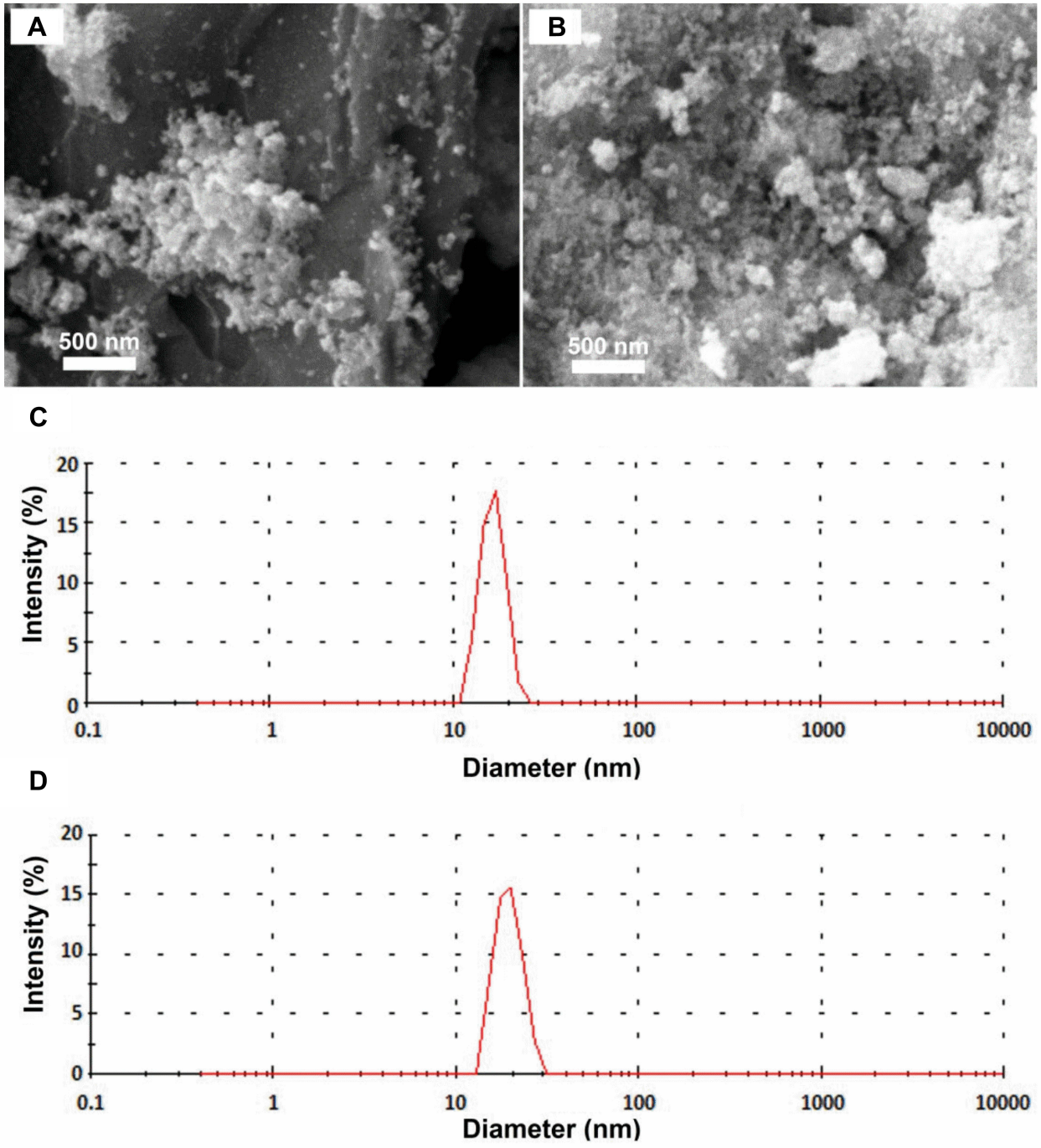

Figure 5 SEM images of (**A**) amine-MNPs and (**B**) MNPs-CMC-DOX. The size distribution of (**C**) amine-MNPs and (**D**) MNPs-CMC-DOX as determined by DLS.

After fitting the release data into different kinetic models, the r^2 values obtained are presented in Table 1. The release profiles of MNPs-CMC-DOX fit both the first-order model and the Higuchi model. The process of agent release, therefore, involves the penetration of PBS into the polymer matrix and the diffusion of DOX molecules from the nanocomposites to the external release medium, with the release rate being directly proportional to the DOX content. In addition, to determine the release mechanism of MNPs-CMC-DOX, 60% of the release data are fitted into the Korsmeyer-Peppas equation. The *n* values are in the range from 0.624 to 0.659, indicating that MNPs-CMC-DOX follows a non-Fickian diffusion mechanism.

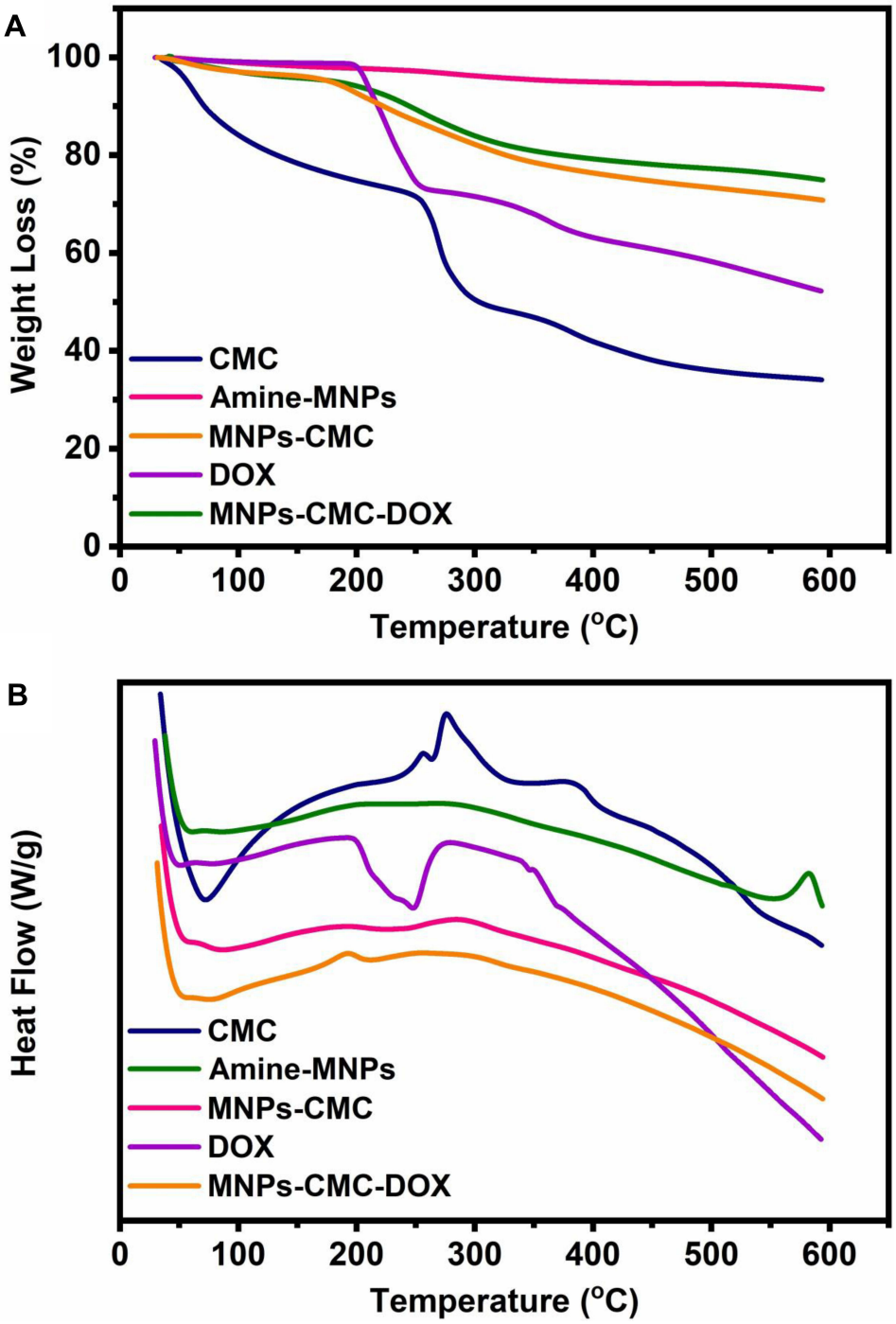

Figure 6 (**A**) TGA and (**B**) DSC curves of CMC, amine-MNPs, MNPs-CMC, DOX, and MNPs-CMC-DOX.

Cytotoxic Effects and ROS-Generating Capacity

The cytotoxic effects of DOX, MNPs-CMC and MNPs-CMC-DOX are tested in MCF-7 human breast cancer cells (Figure 8). This cell line is selected because it is one of the most studied cancer cell lines in the literature for cancer research,[47] and hence can serve as a good model when the effect of our nanocomposites on cancer cells is evaluated. Owing to prolonged release of DOX from the nanocomposites, the cytotoxicity of MNPs-CMC-DOX and MNPs-CMC in MCF-7 cells is lower than that of DOX. A similar observation has been reported by previous studies,[48,49] in which sustained release of a toxic agent has been found to cause a reduction in the observed toxicity.

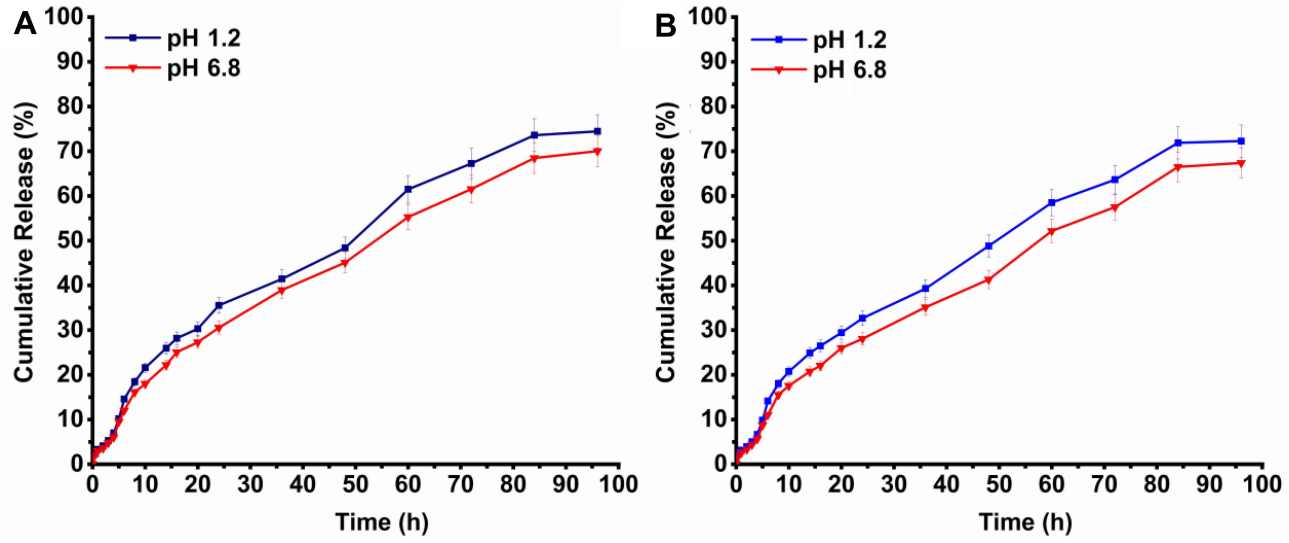

Figure 7 Release patterns of DOX from MNPs-CMC-DOX at (**A**) 37°C and (**B**) 25°C.

After 24 h of cell treatment with MNPs-CMC-DOX (100 μg/mL), the percentage of the viability of cancer cells drops to only 8.3% (Figure 8B). Intriguingly, MNPs-CMC displays toxic effects against MCF-7 cells as well (Figure 8C). This is proposed to be due to the ROS-generating capacity of the nanocomposites. Such hypothesis is confirmed by the increase in the intracellular ROS level of MCF-7 cells after treatment with the nanocomposites (Figure 9A). Apart from using MCF-7 cells, the cytotoxic effects of the nanocomposites are determined in 3T3 fibroblasts (Figure 9B). These cells are selected because their viable rates are substrate-dependent, making them extensively used in the literature to evaluate the cytotoxicity of an agent of interest.[50,51] After treatment with the nanocomposites for 24 h at a concentration as high as 100 μg/mL, over 80% of the cells are still viable. This suggests that the toxicity of nanocomposites varies with the cell type, being highly toxic to MCF-7 cells but showing good biocompatibility with 3T3 fibroblasts.

Conclusion

Nanocomposites enabling controlled delivery of bioactive agents is of practical importance in treatment development.[52–57] This study conjugates amine-MNPs with CMC to generate nanocomposites as carriers of bioactive agents. Although the size of amine-MNPs increases after conjugation with the polymer, the size of the nanocomposites is still in the nanoscale. The release pattern of MNPs-CMC-DOX is examined at different temperatures and pH values. Not only can our nanocomposites serve as pH-responsive carriers for controlled agent release, but they can also ROS-generating capacity to elicit cytotoxic effects. Intriguingly, the cytotoxic effects led by our nanocomposites are cell type-dependent. To facilitate the use of the nanocomposites in treatment development, more studies to examine the effects of various parameters (including the size and shape) on cytotoxicity and ROS-generating capacity, as well as the elucidation of mechanisms underlying the cell type-specific toxicity, are required; however, based on the performance of the nanocomposites as shown in this study, it is anticipated that our nanocomposites will show high practical potential for applications in controlled release of bioactive agents.

Table 1 Release Kinetic Parameters of MNPs-CMC-DOX at Different pH Values (6.8 and 1.2) and Temperatures (37°C and 25°C)

pH	Temperature	Zero-Order Model		First-Order Model		Higuchi Model		Korsmeyer-Peppas Model	
		K_0	r^2	K_1	r^2	K_H	r^2	n	r^2
1.2	37°C	0.940	0.878	0.016	0.977	7.394	0.970	0.618	0.991
	25°C	0.899	0.884	0.015	0.973	7.065	0.968	0.624	0.990
6.8	37°C	0.866	0.904	0.014	0.982	6.769	0.965	0.645	0.994
	25°C	0.823	0.914	0.013	0.980	6.415	0.960	0.659	0.994

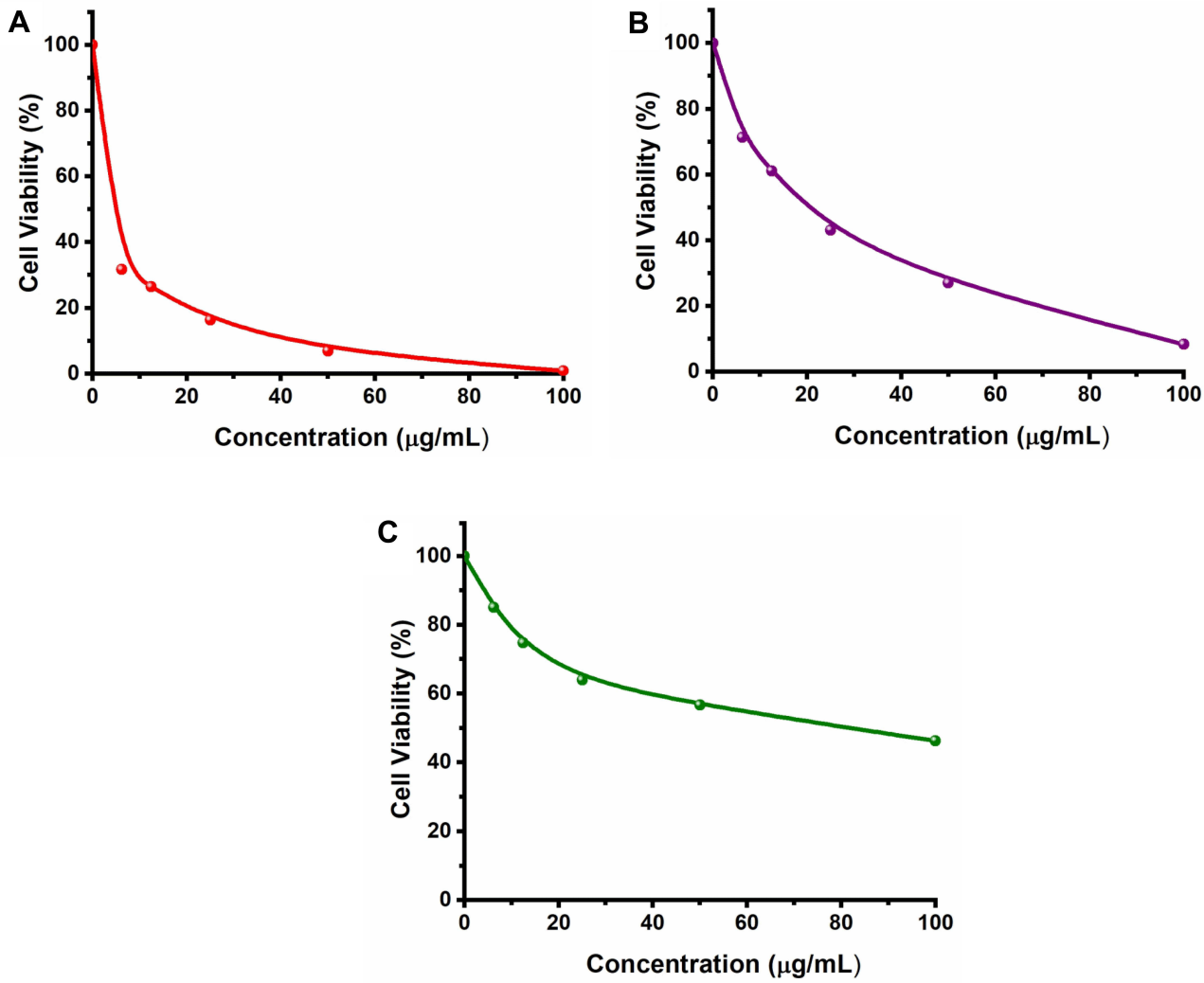

Figure 8 Viability of MCF-7 cells after treatment with (**A**) DOX, (**B**) MNPs-CMC-DOX, and (**C**) MNPs-CMC.

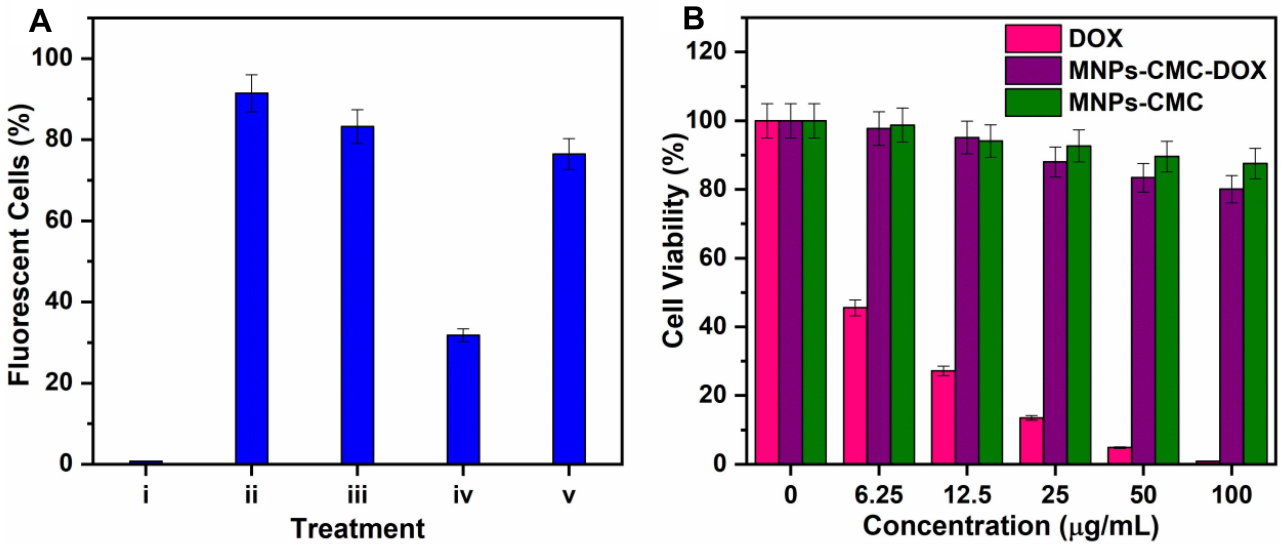

Figure 9 (**A**) Effect of different treatments on the intracellular ROS level of MCF-7 cells as determined by the H_2DCFDA assay: (i) no treatment, (ii) treatment with H_2O_2, (iii) treatment with DOX, (iv) treatment with MNPs-CMC, and (v) treatment MNPs-CMC-DOX. (**B**) Viability of 3T3 cells after treatment with DOX, MNPs-CMC-DOX, and MNPs-CMC.

Disclosure

The authors report no conflicts of interest in this work.

References

1. Jeng HA, Swanson J. Toxicity of metal oxide nanoparticles in mammalian cells. *J Environ Sci Health A*. 2006;41(12):2699–2711. doi:10.1080/10934520600966177
2. Lai WF, Wong WT, Rogach AL. Development of copper nanoclusters for in vitro and in vivo theranostic applications. *Adv Mater*. 2020;32(9):e1906872. doi:10.1002/adma.201906872
3. Sengupta J, Ghosh S, Datta P, et al. Physiologically important metal nanoparticles and their toxicity. *J Nanosci Nanotechnol*. 2014;14(1):990–1006. doi:10.1166/jnn.2014.9078
4. Nel A, Xia T, Mädler L, et al. Toxic potential of materials at the nanolevel. *Science*. 2006;311(5761):622–627. doi:10.1126/science.1114397
5. Sengupta J, Datta P, Patra HK, et al. In vivo interaction of gold nanoparticles after acute and chronic exposures in experimental animal models. *J Nanosci Nanotechnol*. 2013;13(3):1660–1670. doi:10.1166/jnn.2013.7113
6. Park EJ, Kim H, Kim Y, et al. Intratracheal instillation of platinum nanoparticles may induce inflammatory responses in mice. *Arch Pharm Res*. 2010;33(5):727–735. doi:10.1007/s12272-010-0512-y
7. Chen M, von Mikecz A. Formation of nucleoplasmic protein aggregates impairs nuclear function in response to SiO_2 nanoparticles. *Exp Cell Res*. 2005;305(1):51–62. doi:10.1016/j.yexcr.2004.12.021
8. Alarifi S, Ali D, Alakhtani S, et al. Reactive oxygen species-mediated DNA damage and apoptosis in human skin epidermal cells after exposure to nickel nanoparticles. *Biol Trace Elem Res*. 2014;157(1):84–93. doi:10.1007/s12011-013-9871-9
9. Wang Y, Aker WG, Hwang H-M, et al. A study of the mechanism of in vitro cytotoxicity of metal oxide nanoparticles using catfish primary hepatocytes and human HepG2 cells. *Sci Total Environ*. 2011;409(22):4753–4762. doi:10.1016/j.scitotenv.2011.07.039
10. Amani A, Begdelo JM, Yaghoubi H, et al. Multifunctional magnetic nanoparticles for controlled release of anticancer drug, breast cancer cell targeting, MRI/fluorescence imaging, and anticancer drug delivery. *J Drug Deliv Sci Technol*. 2019;49:534–546. doi:10.1016/j.jddst.2018.12.034
11. Sağir T, Huysal M, Durmus Z, et al. Preparation and in vitro evaluation of 5-flourouracil loaded magnetite–zeolite nanocomposite (5-FU-MZNC) for cancer drug delivery applications. *Biomed Pharmacother*. 2016;77:182–190. doi:10.1016/j.biopha.2015.12.025
12. Farazi R, Vaezi MR, Molaei MJ, et al. Effect of pH and temperature on doxorubicin hydrochloride release from magnetite/graphene oxide nanocomposites. *Mater Today Proc*. 2018;5(7, Part 3):15726–15732. doi:10.1016/j.matpr.2018.04.184
13. Alikhanzadeh-Arani S, Almasi-Kashi M, Sargazi S, et al. CoNiZn and CoNiFe nanoparticles: synthesis, physical characterization, and in vitro cytotoxicity evaluations. *Appl Sci*. 2021;11(12):5339. doi:10.3390/app11125339
14. Avval ZM, Malekpour L, Raeisi F, et al. Introduction of magnetic and supermagnetic nanoparticles in new approach of targeting drug delivery and cancer therapy application. *Drug Metab Rev*. 2020;52(1):157–184. doi:10.1080/03602532.2019.1697282
15. Gholami A, Mousavi SM, Hashemi SA. Current trends in chemical modifications of magnetic nanoparticles for targeted drug delivery in cancer chemotherapy. *Drug Metab Rev*. 2020;52(1):205–224. doi:10.1080/03602532.2020.1726943
16. Wilhelm C, Fortin JP, Gazeau F. Tumour cell toxicity of intracellular hyperthermia mediated by magnetic nanoparticles. *J Nanosci Nanotechnol*. 2007;7(8):2933–2937. doi:10.1166/jnn.2007.668
17. Sun C, Lee JSH, Zhang M. Magnetic nanoparticles in MR imaging and drug delivery. *Adv Drug Deliv Rev*. 2008;60(11):1252–1265. doi:10.1016/j.addr.2008.03.018
18. Saravani R, Sargazi S, Saravani R, et al. Newly crocin-coated magnetite nanoparticles induce apoptosis and decrease VEGF expression in breast carcinoma cells. *J Drug Deliv Sci Technol*. 2020;60:101987. doi:10.1016/j.jddst.2020.101987
19. Zhu L, Ma J, Jia N, et al. Chitosan-coated magnetic nanoparticles as carriers of 5-fluorouracil: preparation, characterization and cytotoxicity studies. *Colloids Surf B Biointerfaces*. 2009;68(1):1–6. doi:10.1016/j.colsurfb.2008.07.020
20. Tian J, Yan C, Liu K. Paclitaxel-loaded magnetic nanoparticles: synthesis, characterization, and application in targeting. *J Pharm Sci*. 2017;106(8):2115–2122. doi:10.1016/j.xphs.2017.04.023
21. Prabha G, Raj V. Sodium alginate–polyvinyl alcohol–bovin serum albumin coated Fe3O4 nanoparticles as anticancer drug delivery vehicle: doxorubicin loading and in vitro release study and cytotoxicity to HepG2 and L02 cells. *Mater Sci Eng C*. 2017;79:410–422. doi:10.1016/j.msec.2017.04.075
22. Sung YK, Kim SW. Recent advances in polymeric drug delivery systems. *Biomater Res*. 2020;24(1):12. doi:10.1186/s40824-020-00190-7
23. Lai WF, Susha AS, Rogach AL, et al. Electrospray-mediated preparation of compositionally homogeneous core-shell hydrogel microspheres for sustained drug release. *RSC Adv*. 2017;7(70):44482–44491. doi:10.1039/c7ra07568e
24. Lai WF, Tang R, Wong WT. Ionically crosslinked complex gels loaded with oleic acid-containing vesicles for transdermal drug delivery. *Pharmaceutics*. 2020;12(8):725. doi:10.3390/pharmaceutics12080725
25. Lai WF, Tang GP, Wang X, et al. Cyclodextrin-PEI-Tat polymer as a vector for plasmid DNA delivery to placenta mesenchymal stem cells. *Bionano Sci*. 2011;1(3):89–96. doi:10.1007/s12668-011-0010-9
26. Nishimura SI, Nishi N, Tokura S, et al. Bioactive chitin derivatives. activation of mouse-peritoneal macrophages by O-(carboxymethyl)chitins. *Carbohydr Res*. 1986;146(2):251–258. doi:10.1016/0008-6215(86)85044-3
27. Lai WF. Non-conjugated polymers with intrinsic luminescence for drug delivery. *J Drug Deliv Sci Tech*. 2020;59:101916. doi:10.1016/j.jddst.2020.101916
28. Lai WF, Hu C, Deng G, et al. A biocompatible and easy-to-make polyelectrolyte dressing with tunable drug delivery properties for wound care. *Int J Pharm*. 2019;566:101–110. doi:10.1016/j.ijpharm.2019.05.045
29. Lai WF, Lin MC. Nucleic acid delivery with chitosan and its derivatives. *J Control Release*. 2009;134(3):158–168. doi:10.1016/j.jconrel.2008.11.021
30. Lai WF, Lin MC. Folate-conjugated chitosan-poly (ethylenimine) copolymer as an efficient and safe vector for gene delivery in cancer cells. *Curr Gene Ther*. 2015;15(5):472–480. doi:10.2174/1566523215666150812120347

31. Lai WF, Deng R, He T, et al. A bioinspired, sustained-release material in response to internal signals for biphasic chemical sensing in wound therapy. *Adv Healthc Mater*. 2021;10(2):e2001267. doi:10.1002/adhm.202001267
32. Maeda Y, Kimura Y. Antitumor effects of various low-molecular-weight chitosans are due to increased natural killer activity of intestinal intraepithelial lymphocytes in sarcoma 180–bearing mice. *J Nutr*. 2004;134(4):945–950. doi:10.1093/jn/134.4.945
33. Pae HO, Seo WG, Kim NY, et al. Induction of granulocytic differentiation in acute promyelocytic leukemia cells (HL-60) by water-soluble chitosan oligomer. *Leuk Res*. 2001;25(4):339–346. doi:10.1016/S0145-2126(00)00138-7
34. Yu Z, Zhao L, Ke H. Potential role of nuclear factor-kappaB in the induction of nitric oxide and tumor necrosis factor-alpha by oligochitosan in macrophages. *Int Immunopharmacol*. 2004;4(2):193–200. doi:10.1016/j.intimp.2003.12.001
35. Chi J, Jiang Z, Qiao J, et al. Synthesis and anti-metastasis activities of norcantharidin-conjugated carboxymethyl chitosan as a novel drug delivery system. *Carbohydr Polym*. 2019;214:80–89. doi:10.1016/j.carbpol.2019.03.026
36. Reddy OS, Lai WF. Development of a composite film fabricated from carboxymethyl chitosan and magnetite nanoparticles for pH-responsive bioactive agent release. *Biointerphases*. 2021;16(2):021006. doi:10.1116/6.0000726
37. Bukzem AL, Signini R, dos Santos DM, et al. Optimization of carboxymethyl chitosan synthesis using response surface methodology and desirability function. *Int J Biol Macromol*. 2016;85:615–624. doi:10.1016/j.ijbiomac.2016.01.017
38. Sreekanth Reddy O, Subha MCS, Jithendra T, et al. Curcumin encapsulated dual cross linked sodium alginate/montmorillonite polymeric composite beads for controlled drug delivery. *J Pharm Anal*. 2021;11(2):191–199. doi:10.1016/j.jpha.2020.07.002
39. Gouda R, Baishya H, Qing Z. Application of mathematical models in drug release kinetics of carbidopa and levodopa ER tablets. *J Dev Drugs*. 2017;6(2):1000171. doi:10.4172/2329-6631.1000171
40. Costa P, Lobo JMS. Modeling and comparison of dissolution profiles. *Eur J Pharm Sci*. 2001;13(2):123–133. doi:10.1016/S0928-0987(01)00095-1
41. Obireddy SR, Lai WF. Multi-component hydrogel beads incorporated with reduced graphene oxide for pH-responsive and controlled co-delivery of multiple agents. *Pharmaceutics*. 2021;13(3):313. doi:10.3390/pharmaceutics13030313
42. Nivethaa EAK, Baskar S, Ann Martin C, et al. A competent bidrug loaded water soluble chitosan derivative for the effective inhibition of breast cancer. *Sci Rep*. 2020;10(1):3991. doi:10.1038/s41598-020-60888-5
43. Bhattacharya D, Behera B, Sahu SK, et al. Design of dual stimuli responsive polymer modified magnetic nanoparticles for targeted anti-cancer drug delivery and enhanced MR imaging. *New J Chem*. 2016;40(1):545–557. doi:10.1039/C5NJ02504D
44. Zhu L, Wang D, Wei X, et al. Multifunctional pH-sensitive superparamagnetic iron-oxide nanocomposites for targeted drug delivery and MR imaging. *J Control Release*. 2013;169(3):228–238. doi:10.1016/j.jconrel.2013.02.015
45. Obireddy SR, Chintha M, Kashayi CR, et al. Gelatin-coated dual cross-linked sodium alginate/magnetite nanoparticle microbeads for controlled release of doxorubicin. *ChemistrySelect*. 2020;5(33):10276–10284. doi:10.1002/slct.202002604
46. Verma NK, Purohit MP, Equbal D, et al. Targeted smart pH and thermoresponsiveN, O-carboxymethyl chitosan conjugated nanogels for enhanced therapeutic efficacy of doxorubicin in mcf-7 breast cancer cells. *Bioconjug Chem*. 2016;27(11):2605–2619. doi:10.1021/acs.bioconjchem.6b00366
47. Lee AV, Oesterreich S, Davidson NE. MCF-7 cells-changing the course of breast cancer research and care for 45 years. *J Natl Cancer Inst*. 2015;107(7):73. doi:10.1093/jnci/djv073
48. Boddu A, Obireddy SR, Subbarao SMC, et al. Encapsulation of 5-fluorouracil treated reduced graphene oxide in sodium alginate matrix for controlled and pH-responsive drug delivery. *ChemistrySelect*. 2021;6(25):6533–6540. doi:10.1002/slct.202101395
49. Lai WF, Huang E, Wong WT. A gel-forming clusteroluminogenic polymer with tunable emission behavior as a sustained-release carrier enabling real-time tracking during bioactive agent delivery. *Appl Mater Today*. 2020;21:100876. doi:10.1016/j.apmt.2020.100876
50. Lai WF, Huang E, Lui KH. Alginate-based complex fibers with the Janus morphology for controlled release of co-delivered drugs. *Asian J Pharm Sci*. 2020;16(1):77–85. doi:10.1016/j.ajps.2020.05.003
51. Lai WF, Gui DY, Wong MG, et al. A self-indicating cellulose-based gel with tunable performance for bioactive agent delivery. *J Drug Deliv Sci Tech*. 2021;63:102428. doi:10.1016/j.jddst.2021.102428
52. Ahmadi S, Fazilati M, Mousavi SM, et al. Anti-bacterial/fungal and anti-cancer performance of green synthesized Ag nanoparticles using summer savoury extract. *J Exp Nanosci*. 2020;15(1):363–380. doi:10.1080/17458080.2020.1799981
53. Dong P, Rakesh KP, Manukumar HM, et al. Innovative nano-carriers in anticancer drug delivery-a comprehensive review. *Bioorg Chem*. 2019;85:325–336. doi:10.1016/j.bioorg.2019.01.019
54. Mousavi SM, Low FW, Hashemi SA, et al. Development of graphene based nanocomposites towards medical and biological applications. *Artif Cells Nanomed Biotechnol*. 2020;48(1):1189–1205. doi:10.1080/21691401.2020.1817052
55. De Jong WH, Borm PJA. Drug delivery and nanoparticles: applications and hazards. *Int J NanoMedicine*. 2008;3(2):133–149. doi:10.2147/ijn.s596
56. Rahdar A, Hajinezhad MR, Sargazi S, et al. Deferasirox-loaded pluronic nanomicelles: synthesis, characterization, in vitro and in vivo studies. *J Mol Liq*. 2021;323:114605. doi:10.1016/j.molliq.2020.114605
57. Sargazi S, Hajinezhad MR, Barani M, et al. Synthesis, characterization, toxicity and morphology assessments of newly prepared microemulsion systems for delivery of valproic acid. *J Mol Liq*. 2021;338:116625. doi:10.1016/j.molliq.2021.116625